

Power-law decay of the spatial correlation function in exciton-polariton condensates

Georgios Roumpos^{a,1,2}, Michael Lohse^{a,b}, Wolfgang H. Nitsche^a, Jonathan Keeling^c, Marzena Hanna Szymańska^{d,e}, Peter B. Littlewood^{f,g}, Andreas Löffler^h, Sven Höfling^h, Lukas Worschech^h, Alfred Forchel^h, and Yoshihisa Yamamoto^{a,i}

^aE. L. Ginzton Laboratory, Stanford University, Stanford, CA 94305; ^bFakultät für Physik, Universität Karlsruhe, Karlsruhe 76128, Germany; ^cScottish Universities Physics Alliance, School of Physics and Astronomy, University of St. Andrews, St. Andrews, KY16 9SS, United Kingdom; ^dDepartment of Physics, University of Warwick, Coventry, CV4 7AL, United Kingdom; ^eLondon Centre for Nanotechnology, London, WC1H 0AH, United Kingdom; ^fArgonne National Laboratory, Argonne, IL 60439; ^gJames Franck Institute, University of Chicago, Chicago, IL 60637; ^hTechnische Physik, Universität Würzburg, Physikalisches Institut and Wilhelm-Conrad-Röntgen-Research Center for Complex Material Systems, Würzburg 97070, Germany; and ⁱNational Institute of Informatics, Tokyo 153-8505, Japan

Edited by Peter Zoller, University of Innsbruck, Austria, and approved February 27, 2012 (received for review May 20, 2011)

We create a large exciton-polariton condensate and employ a Michelson interferometer setup to characterize the short- and long-distance behavior of the first order spatial correlation function. Our experimental results show distinct features of both the two-dimensional and nonequilibrium characters of the condensate. We find that the gaussian short-distance decay is followed by a power-law decay at longer distances, as expected for a two-dimensional condensate. The exponent of the power law is measured in the range 0.9–1.2, larger than is possible in equilibrium. We compare the experimental results to a theoretical model to understand the features required to observe a power law and to clarify the influence of external noise on spatial coherence in nonequilibrium phase transitions. Our results indicate that Berezinskii–Kosterlitz–Thouless-like phase order survives in open-dissipative systems.

quantum well excitons | semiconductor microcavities

The spatial correlation function quantifies the coherence properties of a system (1). In a 3D Bose-condensed gas, long range order is observed, and the correlation function decays toward a plateau at large distances (2, 3). In the homogeneous 2D Bose gas (4), however, no long range order can be established (5). Instead, Berezinskii–Kosterlitz–Thouless (BKT) theory of the equilibrium interacting gas predicts a transition to a low-temperature superfluid phase, which shows a power-law decay of the correlation function (6, 7). Unfortunately, it is frequently hard to directly measure this, and only very recently (8) was indication of the power-law decay of coherence seen in a 2D atomic gas. It has been theoretically predicted (9, 10) that power-law decay of coherence survives in the nonequilibrium problem, and it is this prediction that the current experiment sets out to test.

Exciton polaritons are short-lived quasiparticles formed in a semiconductor quantum well strongly coupled to a planar microcavity (11). Each one is a superposition of a quantum well exciton and a microcavity photon, and they behave as 2D bosons below the Mott density. Above a threshold particle density, condensation is observed (12). Due to the nonequilibrium nature of polariton condensation, understanding its coherence properties is quite revealing regarding the different roles of fluctuations in the equilibrium and nonequilibrium problems.

Previous measurements on polariton condensates have demonstrated coherence at large distances but were limited by large experimental uncertainties (13) or highly disordered samples (14, 15), and the long-distance behavior could not be fully extracted. Recently, the correlation function at large distances was studied in 1D condensates confined in a quantum wire (16) and in a valley of the disorder potential (17). In ref. 16, the data was energy-resolved so that excited states were filtered out, while in ref. 17 a rare area on the sample was chosen in which a single mode condensate is seen. The purpose of both those experiments was to investigate how long the coherence length of a spectrally isolated 1D condensate state can be. We, on the other hand, are

interested in the functional form of the correlation function in a 2D condensate and how the excitations populated by the pumping and decay processes can modify it.

With our setup, we can measure values of $g^{(1)}(r)$ as low as 0.02, so we can reliably extract the long-distance behavior. We find that, although true thermal equilibrium is not established, an effective thermal de Broglie wavelength can still be defined from the short-distance gaussian decay of $g^{(1)}(r)$. Furthermore, $g^{(1)}(r)$ at long distances r decays according to a power law, in analogy to the equilibrium BKT superfluid phase. The exponent of the power-law decay is, however, higher than can be possible within the BKT theory. We apply a nonequilibrium theory (9, 10) to identify the source of the large exponent. We argue that, although the spectrum is modified due to dissipation, the exponent would still have the equilibrium value if the spectrum was thermally populated. If, on the other hand, a white noise source acts on the system and induces a flat occupation of the excited states, the exponent can have a large value, proportional to the noise strength. We therefore conclude that the pumping and decay processes, which introduce a nonthermal occupation of the excited states, can be responsible for the large value of the exponent.

Results

In our study, we use a weak-disorder GaAs-based sample, the same one as in our recent experiments (18). The condensate is generated nonresonantly by the multimode laser, which creates free electron-hole pairs at an excitation energy approximately 100 meV above the lower polariton (LP) energy. Carriers suffer multiple scatterings before reaching the LP energy, so coherence is established spontaneously in the condensate and cannot be inherited from the laser pump. The laser is continuously on and replaces LPs that leak out of the microcavity at a ps rate. We are interested in the limit of the homogeneous 2D polariton gas. For this purpose, we employ a setup based on a refractive beam shaper that forms a large laser excitation spot with uniform intensity. There is no confining potential on our sample. Because of the short lifetime, however, the condensate density follows the photon density of the excitation spot, so we can create circular condensates with almost flat density and diameters ranging from 14 μm to 44 μm (see ref. 18 and *SI Appendix*). LP luminescence in the steady state is observed through a combination of a long-pass

Author contributions: P.B.L. and Y.Y. designed research; G.R., M.L., W.H.N., J.K., and M.H.S. performed research; A.L., S.H., L.W., and A.F. contributed new reagents/analytic tools; G.R. and M.L. analyzed data; and G.R. and J.K. wrote the paper.

The authors declare no conflict of interest.

This article is a PNAS Direct Submission.

¹Present address: JILA, University of Colorado, Boulder, CO 80309

²To whom correspondence should be addressed. E-mail: georgios.roumpos@jila.colorado.edu.

This article contains supporting information online at www.pnas.org/lookup/suppl/doi:10.1073/pnas.1107970109/-DCSupplemental.

and a band-pass interference filter, which reject scattered laser light without distorting the LP spectrum.

We confirmed that the sample disorder potential is weak in two ways (see *SI Appendix*). First, the lineshape of the luminescence at low excitation power is Lorentzian, which is characteristic of a homogeneously broadened line. Second, we measured a 2D map of the disorder potential with resolution approximately 1 μm and found that its spatial fluctuations are indeed weaker than the homogeneous broadening and also much weaker than the energy shift due to polariton–polariton interactions. Therefore, we can ignore the sample disorder in our experiment. The condensate is still localized in space, though, following the shape of the laser excitation spot.

The first order spatial correlation function is defined as

$$g^{(1)}(\mathbf{r}_1, t_1; \mathbf{r}_2, t_2) = \frac{\langle \psi_1^\dagger \psi_2 \rangle}{\sqrt{\langle \psi_1^\dagger \psi_1 \rangle \langle \psi_2^\dagger \psi_2 \rangle}} \quad [1]$$

where ψ_i^\dagger and ψ_i are the creation and annihilation field operators at space-time point (\mathbf{r}_i, t_i) . To measure this function, we built a Michelson interferometer setup. A schematic is shown in Fig. 1A. It includes a mirror in one arm, and a right angle prism in the other. We overlap the condensate real-space image with its reflected version, so that fringes similar to that of Fig. 1B are observed on the camera. By changing the length of one interferometer arm, as shown in Fig. 1A, the relative phase of the two beams is shifted. As a result, the intensity measured at one pixel point shows a sinusoidal modulation (Fig. 1C). From the data of Fig. 1C, we extract the phase difference of the two images at a

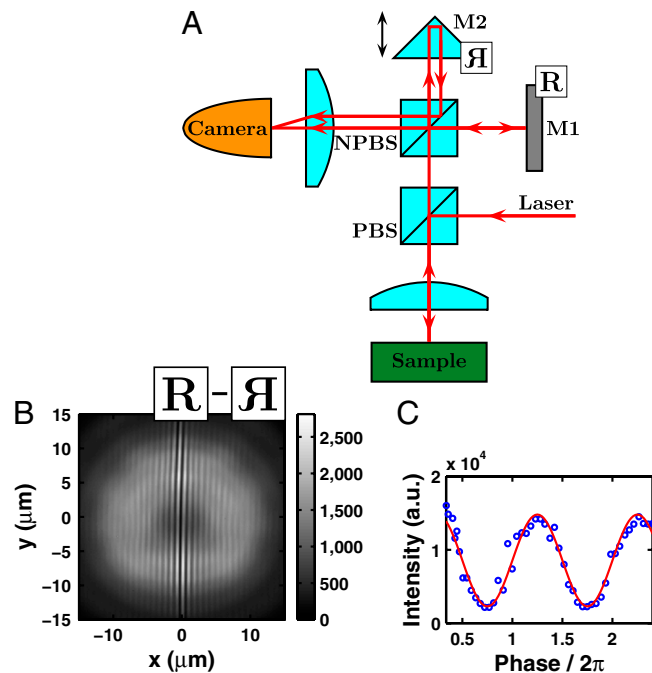


Fig. 1. Michelson interferometer. (A) Schematic of the setup for measurement of the correlation function. The laser is linearly polarized, and we record luminescence of the orthogonal linear polarization through a polarizing beamsplitter (PBS). We then employ a 50-50 nonpolarizing beamsplitter (NPBS), a mirror (M1) and a right-angle prism (M2). The latter creates the reflection of the original image along one axis, depending on the prism orientation. A two-lens microscope setup overlaps the two real space images of the polariton condensate on the camera. (B) Typical interference pattern observed above the polariton condensation threshold along with a schematic showing the orientation of the two overlapping images. (C) Blue circles: measured intensity on one pixel of the camera as a function of the prism (M2) position in normalized units. Red line: fitting to a sine function.

particular pixel point, as well as the fringe visibility. The latter is proportional to the first order correlation function, which is the physical quantity we are interested in in this experiment.

The prism M2 in Fig. 1A forms the reflection of the condensate image along the prism axis. Therefore, point (x, y) overlaps with either $(-x, y)$, or $(x, -y)$ on the camera, depending on the orientation of the prism. This allows us to measure

$$g^{(1)}(x, -x; \tau) \equiv \langle g^{(1)}(x, y, t + \tau; -x, y, t) \rangle_t, \quad [2]$$

or

$$g^{(1)}(y, -y; \tau) \equiv \langle g^{(1)}(x, y, t + \tau; x, -y, t) \rangle_t, \quad [3]$$

where $\langle \rangle_t$ denotes time average. In this experiment, we are mainly interested in interference at $\tau = 0$, so when the time argument is not mentioned explicitly, we imply $\tau = 0$.

We repeat the procedure explained in Fig. 1 for every pixel, so that we measure the phase difference between the two interfering images in addition to the correlation function across the whole spot. Representative data are shown in Fig. 2. Recording both these quantities allows us to identify useful signal from systematic or random noise. Because the prism displaces the beam that is incident on it, the images from the mirror and the prism are focused on the camera from different angles, so the two phase fronts are tilted with respect to each other. As a consequence, we expect to measure a constant phase tilt. This is the case in Fig. 2B, in which the laser power is above threshold and a condensate has formed. We conclude that our measurement of the correlation function in Fig. 2D is reliable over this whole area. On the other hand, at a pump rate below threshold, only short-range correlations exist. Fig. 2A shows that in this case the phase difference is measured correctly only over a small area around the center, ($|x| \leq 1 \mu\text{m}$). So the measured values of $g^{(1)}(x, -x)$ outside this area are not reliable and give an estimate of our measurement uncertainties. As is clear from Fig. 2C, the experimental error can be suppressed down to 0.01.

Phase maps such as those in Fig. 2 have been used to identify localized phase defects—namely, quantum vortices (19). The data of Fig. 2B show that such localized defects are not present in our sample. At points with large fringe visibility (near $x = 0 \mu\text{m}$), fringes are perfectly parallel, whereas defects that appear for large $|x|$ could be due to a numerical uncertainty in the measurement of the local phase due to the small fringe visibility. In any case, localized stationary phase defects cannot influence $g^{(1)}(r)$, because it is their motion that destroys spatial correlations and not their mere presence. It has been found that vortices appear in large disorder samples (19), when a direct external perturbation is introduced (20), before the condensate reaches its steady state (21), or when the condensate moves against an obstacle (22, 23). None of these conditions is satisfied in our experiment. On the other hand, we have found that, under the same conditions as the current experiment, mobile bound vortex pairs appear spontaneously due to the special form of the pumping spot and the pumping and decay noise (18). In ref. (18), we found that a single mobile bound vortex–antivortex pair is visible in a small condensate. In the current experiment, we probe larger condensate sizes, so it is likely that several vortex pairs are present at the same time. Mobile bound vortex pairs are in general invisible in time-integrated phase maps, like the one in Fig. 2B, and they are consistent with a power-law decay of $g^{(1)}(r)$.

Fig. 3A shows the short-distance dependence of $g^{(1)}(x, -x)$ for the same pumping power as in Fig. 2A and C. Every dot in Fig. 3A corresponds to one pixel on the camera, and the x axis is its distance from the axis of reflection (slightly tilted with respect to the columns of the charge-coupled device array). Data at distances $|x| > 1 \mu\text{m}$ is noise, because the measured phase in this area is random (Fig. 24). At shorter distances, we can measure $g^{(1)}(x, -x)$ reliably, and we find that the correlation function has a

Discussion

In ref. 31, it was found that excitation with a low-noise single mode laser revealed the formation of multimode condensation, and the different condensate modes could be spectrally separated. The authors of ref. 31 argued that, if one wants to measure the intrinsic linewidth of polariton condensates, single mode laser excitation and energy-resolved data are required. Indeed, it has been shown (32) that the temporal coherence properties can be understood based on the idea that laser intensity noise introduces population fluctuations, which modulate the interaction energy accordingly, leading to decoherence. However, it is not clear how pump and decay noise influences spatial coherence. Under single mode laser excitations, and when the lowest-energy state is spectrally isolated, long coherence lengths can be observed (15–17, 33). In the current experiment, we are interested in how robust spatial correlations are when excitations are included. We study the “worst case” scenario of multimode laser excitation, which gives broader spectra compared to single mode laser. However, as shown in *SI Appendix*, single mode laser excitation gives similar results in energy-integrated data. We note that laser phase noise cannot be an issue in our experiment, because the laser energy is approximately 100 meV above the LP energy, so the generated quasiparticles suffer multiple scatterings before forming the condensate.

Focusing on the multimode laser excitation case, let us now explore the interpretation of the power law that we observe and consider what it means for the properties of the nonequilibrium polariton condensate. In particular, we discuss under what conditions a power-law decay should be seen and what may control the value and pump power dependence of the observed exponent. As has been discussed previously (9, 10, 34), power-law decay of spatial correlations are not an artifact of equilibrium condensates but survive more generally in a nonequilibrium condensate. Because the power-law decay at long distances arises from the long wavelength collective modes, this statement is not trivial, because dissipation can modify the spectrum at long wavelengths (9, 10, 34).

Let us first recall the results that would apply if one were to consider an equilibrium interacting 2D Bose gas. In this case, the exponent is given by $a_p = 1/n_s \lambda^2 \leq 1/4$, where n_s is the superfluid density and λ is the thermal de Broglie wavelength $\lambda = \sqrt{2\pi\hbar^2/mk_B T}$. The restriction $a_p < 1/4$ occurs because increasing temperature has two effects: It excites long wavelength phase fluctuations, which are responsible for the power-law decay, and it can also excite vortex pairs. The maximum value of a_p occurs at the transition when vortex–antivortex pairs unbind, so that vortices would proliferate, and cause the BKT transition to a phase with short-range correlations. The observation here of a power law $a_p > 1/4$ implies that effects beyond thermal equilibrium are required to explain the data; i.e. there is noise that excites phase fluctuations without leading to vortex proliferation. In addition, because the equilibrium exponent $a_p \propto 1/n_s$, one would expect the exponent to decrease with pump power, as the condensate density increases; the absence of such a decrease again implies effects beyond thermal equilibrium are relevant and suggests that pumping noise is indeed affecting the observed exponent.

Whereas the existence of power-law decay in a nonequilibrium condensate was discussed previously, the value of the exponent and its pump power dependence were not given in those previous works. Using the formalism described in refs. 9 and 10, the exponent can be found by calculating

$$g_1(\Delta\vec{x}) \propto \exp\left[\int \frac{d^2k}{(2\pi)^2} (1 - e^{i\vec{k}\cdot\Delta\vec{x}}) f(k)\right] \quad [4]$$

where $f(k) = \int (d\omega/2\pi) i(D_{\phi\phi}^K - D_{\phi\phi}^R + D_{\phi\phi}^A)$, and $D_{\phi\phi}^{K,R,A}(k, \omega)$ are the Keldysh, retarded, and advanced Green's functions for

phase fluctuations. The advantage of writing the correlation function in this formal way is that it allows one to disentangle the effects of changes to the spectrum of long wavelength excitations from the effects of how this spectrum is populated.

The retarded and advanced Green's functions are independent of how the spectrum is occupied, and following quite general arguments (9, 10, 34) we can prove that they have poles describing the low energy spectrum $\omega_k \simeq -i\gamma \pm \sqrt{\epsilon_k(\epsilon_k + 2\mu) - \gamma^2}$ where $\epsilon_k = \hbar^2 k^2/2m$ is the long wavelength polariton dispersion, μ the chemical potential (or blueshift) and γ is the linewidth.[†] Despite the modification of the equilibrium spectrum introduced by γ , it nevertheless remains the case that if this spectrum is occupied thermally (i.e., if the Keldysh Green's function is chosen to obey the equilibrium fluctuation dissipation theorem), one finds[†]

$$f_{\text{thermal}}(k) \simeq \frac{1}{n_s} \int \frac{d\omega}{2\pi} \frac{4\gamma\mu k_B T}{|\omega^2 + 2i\gamma\omega - 2\mu\epsilon_k|^2} \simeq \frac{mk_B T}{n_s \hbar^2 k^2}, \quad [5]$$

which is independent of γ and matches the equilibrium form of $f(k)$. Thus, despite the modifications to the long wavelength spectrum, a sufficiently thermalized polariton condensate has the equilibrium exponent.

In order to explain the larger exponent observed, and the flat dependence on pump power, we consider a crude model of a system with excess pumping noise as an opposite extreme to the thermalized case. We thus consider a case where the occupation of excitations is set by a Markovian noise source of strength ζ . Namely, we take the inverse Keldysh Green's function to be energy independent.[†] This differs significantly from thermal noise correlations, which are frequency dependent, and diverge at the chemical potential. The measured spectra shown in *SI Appendix* are broad and their linewidth increases as the pumping power is increased. This occupation of excited states could be induced by an energy-independent noise source whose strength increases with the pumping power. In this case, the function $f(k)$ is given by

$$f_{\text{noise}}(k) \simeq \frac{1}{n_s} \int \frac{d\omega}{2\pi} \frac{2\zeta(\mu^2 + \gamma^2)}{|\omega^2 + 2i\gamma\omega - 2\mu\epsilon_k|^2} \quad [6]$$

which, despite the changed occupation spectrum, still yields a power-law decay. The exponent becomes $a_p = (m\zeta/2\pi\hbar^2 n_s) [(\mu^2 + \gamma^2)/2\mu\gamma]$. Because this has the form $a_p \propto \zeta/n_s$ then if the noise strength and polariton density both increase with the pump power, then this would explain the absence of a $1/n_s$ decrease of the exponent, as seen on Fig. 6C.

One point not addressed so far regards the process of vortex proliferation in a noisy nonequilibrium condensate. As pump noise increases, it is likely eventually to lead to proliferation of vortices, and a transition to a state with only short-range correlations, just as occurs at high temperatures in equilibrium.

In conclusion, the measured power-law decay of the correlation function suggests that some form of the BKT superfluid phase survives in nonequilibrium condensates; namely, phase fluctuations are excited but no vortices. The large value of the exponent implies that, in the current experiment, this ordered phase is more robust against external noise than would be expected in equilibrium, in which equipartition holds. We conjecture that the main noise source is pump and decay noise, which create a nonthermal occupation of excited states, and apply a nonequilibrium theory to show that a power-law decay with a large exponent is possible in an open system with excess noise. One may anticipate that sufficient noise could induce vortex proliferation and a transition to short-range coherence. This

[†]See *SI Appendix* for further details.

fascinating possibility remains an open question for future studies.

Materials and Methods

Our GaAs-based sample shows a Rabi splitting of $2\hbar\Omega_{\text{Rabi}} = 14$ meV and LP lifetime of $\tau_{\text{LP}} \sim 2\text{--}4$ ps near photon-exciton detuning $\delta = 0$, where the data presented in this paper is taken. From the curvature of the measured energy versus momentum dispersion at low pumping power, the LP effective mass was found to be $m^* = 9.5 \times 10^{-5} m_e$ at this detuning, where m_e is the electron rest mass. The sample is the same as in our recent experiments (18, 33), and the experimental setup is very similar to ref. 18. We pump the system with a multimode Ti-Sapphire laser operated in the continuous wave mode, combined with a chopper that creates 0.5-ms pulses at 100-Hz repetition rate. All powers quoted in the text and *SI Appendix* refer to the unchopped laser

beam. We employ a commercial refractive beam shaper to generate a flat-top pumping profile of varying size. The Michelson interferometer consists of a 50-50 nonpolarizing cube beamsplitter, a dielectric mirror in the first arm, and an uncoated glass right angle prism in the second one. The position of the prism is controlled by a combination of a translation stage and a piezoelectric actuator.

ACKNOWLEDGMENTS. We acknowledge support from National Science Foundation Grant ECCS-09 25549, Navy/SPAWAR Grant N66001-09-1-2024, FIRST, MEXT, Special Coordination Funds for Promoting Science and Technology, EPSRC, Department of Energy support under FWP 70069, and the State of Bavaria. G.R. thanks M. D. Fraser, F. M. Marchetti, I. Carusotto, and F. Amet for helpful discussions.

1. Chaikin PM, Lubensky TC (2000) *Principles of Condensed Matter Physics* (Cambridge Univ Press).
2. Pitaevskii L, Stringari S (2003) *Bose-Einstein Condensation* (Oxford Univ Press).
3. Bloch I, Hänsch TW, Esslinger T (2000) Measurement of the spatial coherence of a trapped Bose gas at the phase transition. *Nature* 403:166–170.
4. Hadzibabic Z, Dalibard J (2011) Two-dimensional Bose fluids: An atomic physics perspective. *Rivista del Nuovo Cimento* 34:389.
5. Hohenberg PC (1967) Existence of long-range order in one and two dimensions. *Phys Rev* 158:383–386.
6. Berezinskii VL (1972) Destruction of long-range order in one-dimensional and two-dimensional systems possessing a continuous symmetry group. ii. quantum systems. *Sov Phys JETP-USSR* 34:1144–1156.
7. Kosterlitz JM, Thouless DJ (1973) Ordering, metastability and phase transitions in two-dimensional systems. *J Phys C Solid State* 6:1181–1203.
8. Hadzibabic Z, Krüger, Cheneau M, Battelier B, Dalibard J (2006) Berezinskii-Kosterlitz-Thouless crossover in a trapped atomic gas. *Nature* 441:1118–1121.
9. Szymańska MH, Keeling J, Littlewood PB (2006) Nonequilibrium quantum condensation in an incoherently pumped dissipative system. *Phys Rev Lett* 96:230602.
10. Szymańska MH, Keeling J, Littlewood PB (2007) Mean-field theory and fluctuation spectrum of a pumped decaying Bose-Fermi system across the quantum condensation transition. *Phys Rev B Condens Matter Mater Phys* 75:195311.
11. Weisbuch C, Nishioka M, Ishikawa A, Arakawa Y (1992) Observation of the coupled exciton-photon mode splitting in a semiconductor quantum microcavity. *Phys Rev Lett* 69:3314–3317.
12. Deng H, Haug H, Yamamoto Y (2010) Exciton-polariton Bose-Einstein condensation. *Rev Mod Phys* 82:1489–1537.
13. Deng H, Solomon GS, Hey R, Ploog KH, Yamamoto Y (2007) Spatial coherence of a polariton condensate. *Phys Rev Lett* 99:126403.
14. Kasprzak J, et al. (2006) Bose-Einstein condensation of exciton-polaritons. *Nature* 443:409–414.
15. Krizhanovskii DN, et al. (2009) Coexisting nonequilibrium condensates with long-range spatial coherence in semiconductor microcavities. *Phys Rev B Condens Matter Mater Phys* 80:045317.
16. Wertz E, et al. (2010) Spontaneous formation and optical manipulation of extended polariton condensates. *Nat Phys* 6:860–864.
17. Manni F, et al. (2011) Polariton condensation in a one-dimensional disordered potential. *Phys Rev Lett* 106:176401.
18. Roumpos G, et al. (2011) Single vortex-antivortex pair in an exciton polariton condensate. *Nat Phys* 7:129–133.
19. Lagoudakis KG, et al. (2008) Quantized vortices in an exciton-polariton condensate. *Nat Phys* 4:706–710.
20. Tosi G, et al. (2011) Onset and dynamics of vortex-antivortex pairs in polariton optical parametric oscillator superfluids. *Phys Rev Lett* 107:036401.
21. Lagoudakis KG, et al. (2011) Probing the dynamics of spontaneous quantum vortices in polariton superfluids. *Phys Rev Lett* 106:115301.
22. Amo A, et al. (2011) Polariton superfluids reveal quantum hydrodynamic solitons. *Science* 332:1167–1170.
23. Nardin G, et al. (2011) Hydrodynamic nucleation of quantized vortex pairs in a polariton quantum fluid. *Nat Phys* 7:635–641.
24. Weiner AM (2009) *Ultrafast Optics* (John Wiley & Sons, Hoboken, NJ).
25. Wouters M, Carusotto I, Ciuti C (2008) Spatial and spectral shape of inhomogeneous nonequilibrium exciton-polariton condensates. *Phys Rev B Condens Matter Mater Phys* 77:115340.
26. Bajoni D, et al. (2008) Polariton laser using single micropillar GaAs-GaAlAs semiconductor cavities. *Phys Rev Lett* 100:047401.
27. Balili R, Nelsen B, Snoke DW, Snoke L, West K (2009) Role of the stress trap in the polariton quasiequilibrium condensation in GaAs microcavities. *Phys Rev B Condens Matter Mater Phys* 79:075319.
28. Keeling J, Eastham PR, Szymanska MH, Littlewood PB (2005) BCS-BEC crossover in a system of microcavity polaritons. *Phys Rev B Condens Matter Mater Phys* 72:115320.
29. Byrnes T, Horikiri T, Ishida N, Yamamoto Y (2010) BCS wave-function approach to the BEC-BCS crossover of exciton-polariton condensates. *Phys Rev Lett* 105:186402.
30. Klaers J, Schmitt J, Vewinger F, Weitz M (2010) Bose-Einstein condensation of photons in an optical microcavity. *Nature* 468:545–548.
31. Love APD, et al. (2008) Intrinsic decoherence mechanisms in the microcavity polariton condensate. *Phys Rev Lett* 101:067404.
32. Whittaker DM, Eastham PR (2009) Coherence properties of the microcavity polariton condensate. *EPL* 87:27002.
33. Roumpos G, Nitsche WH, Höfling S, Forchel A, Yamamoto Y (2010) Gain-induced trapping of microcavity exciton polariton condensates. *Phys Rev Lett* 104:126403.
34. Wouters M, Carusotto I (2006) Absence of long-range coherence in the parametric emission of photonic wires. *Phys Rev B Condens Matter Mater Phys* 74:245316.

Power-law decay of the spatial correlation function in exciton-polariton condensates Supplementary Information

Georgios Roumpos^{1,8}, Michael Lohse^{1,2}, Wolfgang H. Nitsche¹, Jonathan Keeling³, Marzena Hanna Szymańska⁴, Peter B. Littlewood⁵, Andreas Löffler⁶, Sven Höfling⁶, Lukas Worschech⁶, Alfred Forchel⁶ and Yoshihisa Yamamoto^{1,7}

¹ E. L. Ginzton Laboratory, Stanford University, Stanford, CA 94305, USA

² Fakultät für Physik, Universität Karlsruhe, Karlsruhe 76128, Germany

³ Scottish Universities Physics Alliance, School of Physics and Astronomy, University of St. Andrews, St Andrews KY16 9SS, UK

⁴ Department of Physics, University of Warwick, Coventry CV4 7AL, UK, and London Centre for Nanotechnology, London WC1H 0AH, UK

⁵ Argonne National Laboratory, Argonne, IL 60439, USA, and James Franck Institute, University of Chicago, IL 60637, USA

⁶ Technische Physik, Universität Würzburg, Physikalisches Institut and Wilhelm-Conrad-Röntgen-Research Center for Complex Material Systems, Würzburg 97070, Germany

⁷ National Institute of Informatics, Tokyo 153-8505, Japan

⁸ Present address: JILA, University of Colorado at Boulder, Boulder, CO 80309, USA

1 Experimental details

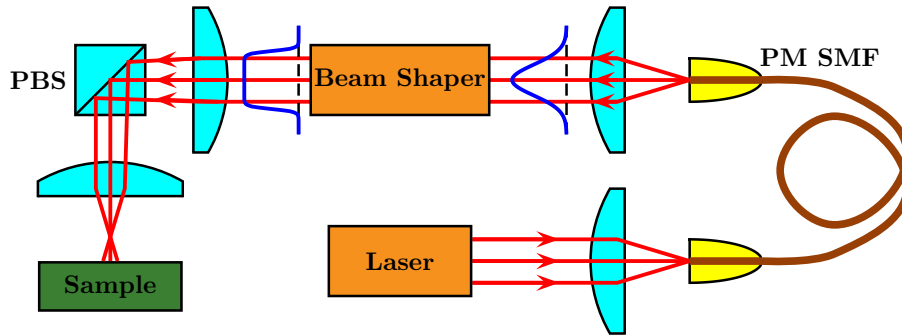


Figure S1: Schematic of the laser pumping setup.

The pumping spot setup is shown in Fig. S1. The laser is first coupled to a polarization-maintaining single mode fiber, and a collimated gaussian beam is created at the other end. The beam is then coupled to a commercial refractive beam shaper, which transforms a collimated gaussian beam of a particular size to a top-hat profile. The objective lens needs to be focused with respect to the sample, since we image the system through it. We can use an extra lens just after the beam shaper, in order

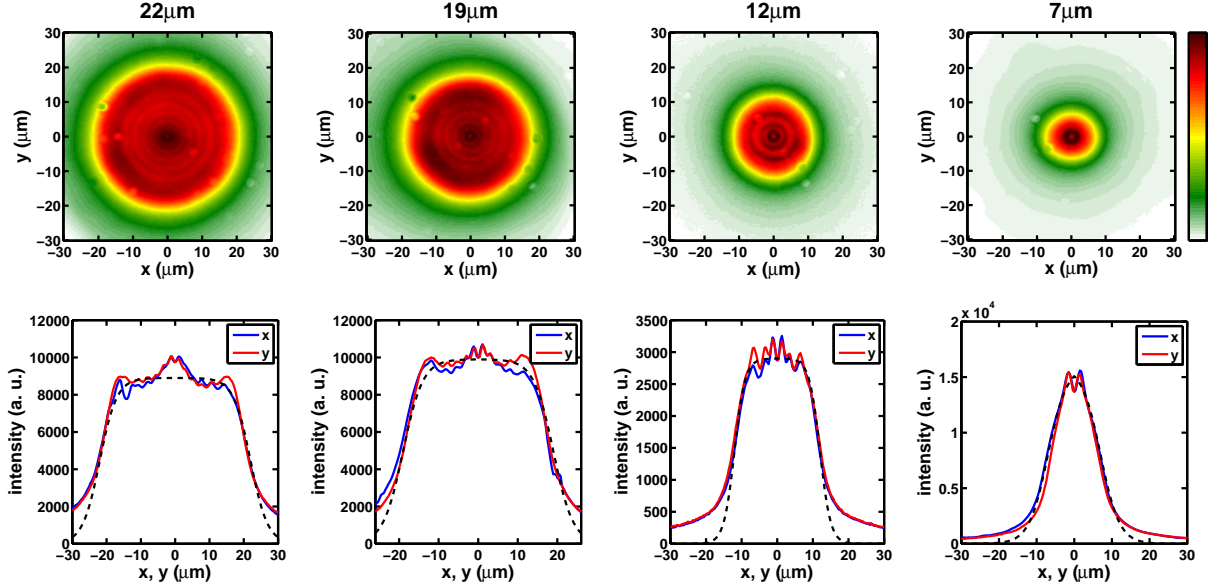


Figure S2: By changing the lens just after the beam shaper in Fig. S1, the pumping spot size can be varied. On the upper row, we plot the LP luminescence images below threshold for the four different spot sizes used in this experiment. The colorscale is linear, and the label on top of every figure is the spot radius. On the lower row, we plot the corresponding 1D profiles along the x - and y -axes. The dashed line is an empirical fit to a Fermi-Dirac function, from which we determine the size of the pumping spot.

to move the focusing point of the laser beam away from the sample surface, and have a large pumping spot on the sample. The focal length of this lens determines the size of the pumping spot. In Fig. S2, we plot LP luminescence images for the four different spot sizes used in this experiment. The pumping power is $\sim 10mW$, which is below the threshold power P_{th} for all four spots.

In Fig. S3, we plot the real space images of LP luminescence for various laser pumping powers, both below and above threshold. We use a combination of two interference filters, one longpass at $750nm$, and one bandpass at $770 \pm 5nm$, which block the laser wavelength without distorting the LP luminescence spectrum. For very low pumping power, luminescence has a top-hat shape. Close to the threshold power of $55mW$, the relaxation rate increases because of enhanced bosonic scattering into the final state. Therefore, the diffusion length shortens, and luminescence takes the shape of the laser excitation spot. Airy-like patterns appear because of diffraction. Above threshold, the condensate progressively takes a doughnut-like shape. We studied this effect in [1], and concluded that the reservoir has a complementary profile with a density maximum at the center and that repulsive condensate-reservoir interactions render this distribution stable. Also, the condensate is smaller than the original spot size because of repulsive LP-LP interactions. In particular, the large condensate density creates an antitrapping potential that pushes LP's away from the center. This effect only influences LP's close to the edge for our top-hat

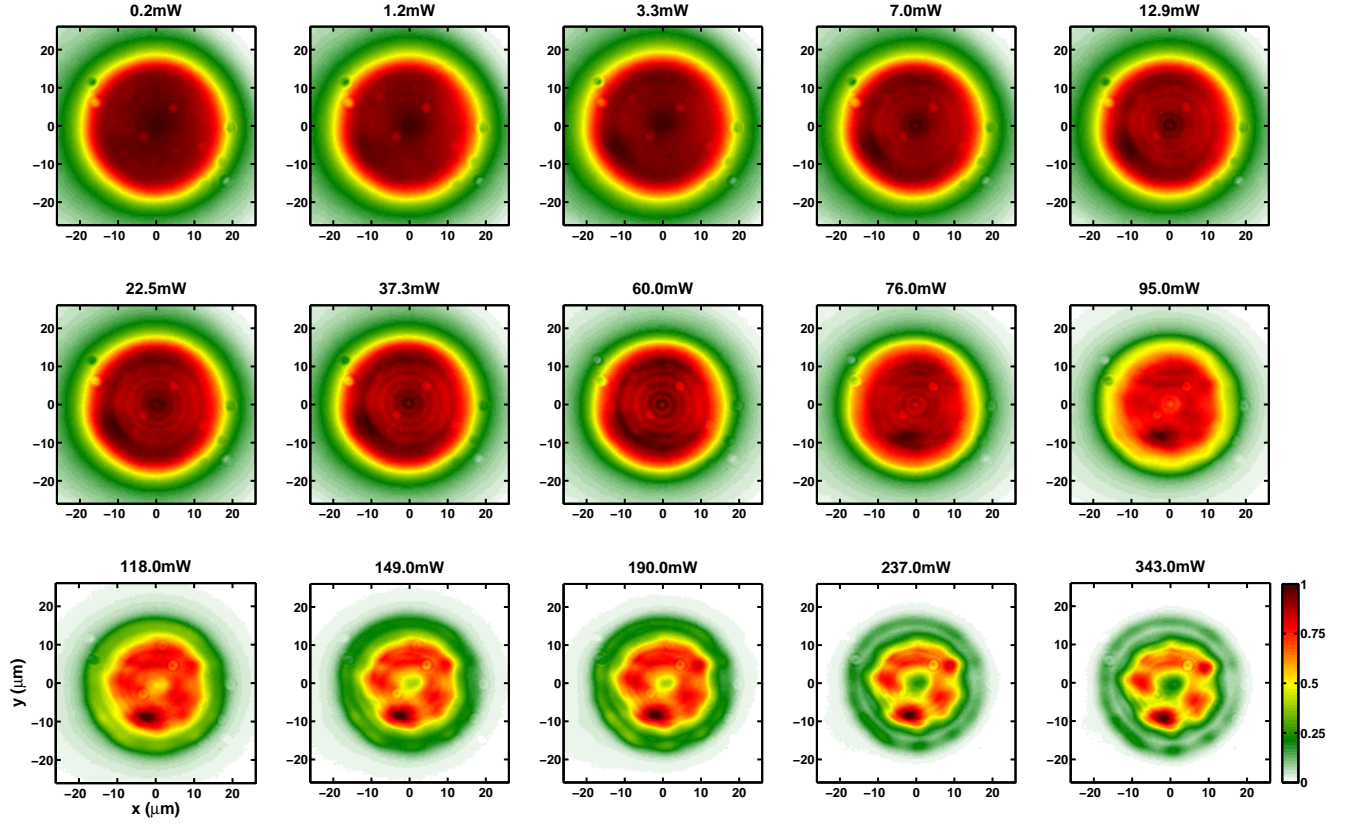


Figure S3: Real space images of LP luminescence for increasing pumping power. Condensation threshold is at $55mW$.

pumping spot.

It is known that the excitation laser spot shape influences the condensation characteristics. In particular, for a small gaussian excitation spot, the condensate ballistically expands due to repulsive polariton-polariton interactions. In this case, condensation occurs in a state with non-zero momentum [2, 3, 4]. Our pumping spot was engineered to probe the limit of the 2D homogeneous polariton gas.

In Fig. S4, we plot momentum space (far field) spectra for a large pumping spot size ($19\mu m$ diameter, same as in Fig. S3). Just above the threshold pumping power, the condensate is formed near zero momentum, and its spectrum blue shifts and broadens as the pumping power is increased.

To estimate up to what extent the sample disorder influences our results, we performed two measurements. In Figure S5a, we show a luminescence spectrum measured at low polariton densities at zero momentum, namely at zero collection angle. To characterize the lineshape, we fit both a Lorentzian and a Gaussian. The Lorentzian fits the data better, which confirms that luminescence is homogeneously broadened. In Figure S5b, we show a map of the sample disorder potential with resolution of

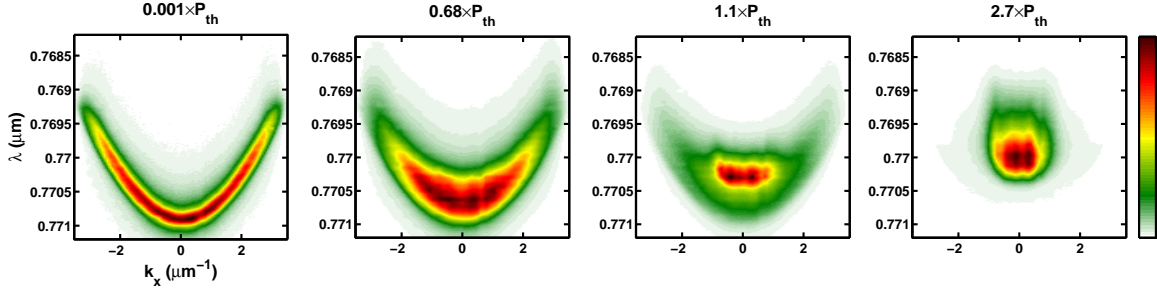


Figure S4: Momentum space (far field) spectra for the $19\mu\text{m}$ diameter pumping spot at different pumping powers in linear color scale (arbitrary units).

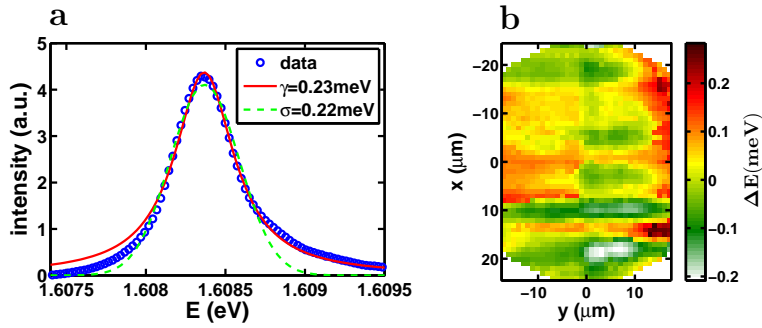


Figure S5: (a) Blue circles: Luminescence spectrum acquired at low pumping power ($\sim 0.015 \times P_{th}$) and at zero momentum. Red continuous line is a fit to a Lorentzian, while green dashed line is a fit to a gaussian. (b) (from [1], Supplementary Information) Map of the disorder potential with spatial resolution of $\sim 1\mu\text{m}$. The sample area pictured here is approximately where the data in the main text was taken.

$\sim 1\mu m$ (see Supplementary Information in [1] for details). The fluctuations of the local disorder potential are smaller than the homogeneous broadening, and much smaller than the condensate blue shift due to repulsive polariton-polariton interactions of $\sim 1meV$. Therefore, for our experiment, we can consider our sample as disorder-free.

The Michelson interferometer setup is described in the main text. Here, we note that the resolution limit of the imaging optics is $\sim 1\mu m$, which influences the measurement of λ_{eff} at small pumping power (see Fig. 2(b) of the main text). If the transfer function of our imaging system is gaussian (namely, if a delta function is imaged to a gaussian) with width λ_{res} , then the measured width of the gaussian decay is $\lambda_{meas} = \sqrt{\lambda_{res}^2 + \lambda_{eff}^2}$, where λ_{eff} is the real effective thermal wavelength, and λ_{meas} is the measured value. Therefore, if the real λ_{eff} is similar to λ_{res} , then the measured λ_{meas} should be close to λ_{res} . The height of the gaussian (unity for a perfect optical system) should also drop to a lower value, so that the total surface does not change. From the measured height of the gaussian fits, namely $g^{(1)}(0, 0) \sim 0.7 - 0.8$, and the measured $\lambda_{meas} \sim 1.6 - 1.7\mu m$, we estimate a lower bound for the real $\lambda_{eff} \geq 1.3\mu m$ at small pumping power.

We can also vary the path length difference between the two arms of the Michelson interferometer. This way, we can measure $g^{(1)}(x, -x; t)$ for various time delays t and probe the temporal coherence of the system. Due to time-integrated detection, the measured coherence time in our experimental setup is mainly influenced by inhomogeneous broadening. Namely, the condensate energy randomly fluctuates in time, and limits the measured fringe visibility. Below the condensation threshold, we observe the interference pattern shown in Fig. 4a of the main text, where the measured visibility $g^{(1)}(x, -x; t)$ is plotted as a function of the time delay t and the distance x from the symmetry axis. At $t = 0$, $g^{(1)}(x, -x; t)$ as a function of x has a gaussian form, as explained in the main text. However, for increasing time delay t , it broadens and acquires an unusual peak structure with multiple maxima and minima.

This can be explained by the fact that the first-order correlation function of a uniform, statistically stationary electromagnetic field is given by the Fourier transform of its power spectrum in momentum space $S(\mathbf{k}, \omega)$ [5]. Below threshold, the observed spectrum can be approximated by

$$S(\mathbf{k}, \omega) = n(\hbar\omega) \frac{\gamma/\pi}{\left(\hbar\omega - \hbar\omega_0 - \frac{\hbar^2|\mathbf{k}|^2}{2m^*}\right)^2 + \gamma^2}, \quad (1)$$

where $\hbar\omega_0$ is the LP resonance at $k = 0$, m^* is the effective mass, γ is the half width at half maximum and $n(\hbar\omega)$ is the particle energy distribution. It is clear that $S(\mathbf{k}, \omega)$ cannot be written in separable form $f(\mathbf{k})g(\omega)$, so the temporal and spatial correlations of $g^{(1)}(x, -x; t)$ are not independent of each other. Therefore the significant occupation of excited states with finite momenta causes a broadening of $g^{(1)}(\Delta x)$ with increasing time delay due to the interference from multiple states with different energies. The internal structure of this broadened peak with multiple local minima and maxima results from the sharp cutoff in the far-field spectrum. The sharp cutoff is due to the fact that the polariton distribution is non-thermal because of the short lifetime and because the polariton lifetime changes as LP's become more and more exciton-like at larger wavevectors. This effect is similar to the diffraction pattern of light created by sharp-edged objects like a slit.

To demonstrate this, we measured the far-field spectrum well below threshold (Fig 4(b) of the main text) and calculated its Fourier transform (Fig 4(c) of the main text) which shows a behavior very similar to the one observed for the experimentally measured correlation function. Although this effect makes the exact determination of the dephasing time and even its definition

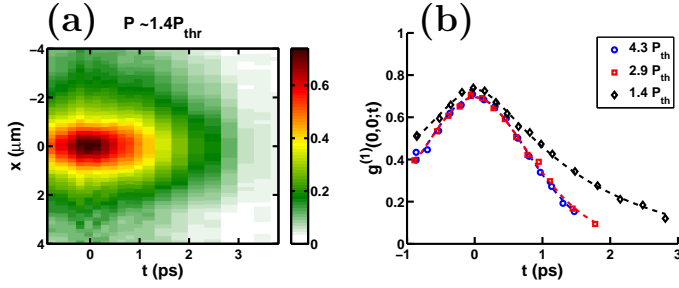


Figure S6: (a) Measured $g^{(1)}(x, -x; t)$ above threshold. (b) $g^{(1)}(0, 0; t)$ for different pumping powers above threshold. Dashed lines are fits using equation (2)

Table 1: Parameters of the fitting lines in Fig. S6(b) based on equation (2).

P/P_{thr}	τ_r (ps)	τ_c (ps)
1.4	0.3	1.0
2.9	1.2	1.0
4.3	2.0	1.1

impossible, one can still conclude that the correlations decay on a very fast timescale, smaller than or similar to the polariton lifetime of 2-4ps

Above threshold, the shape of $g^{(1)}(x, -x; t)$ changes significantly (Fig. S6(a)). The broadening is very weak and the internal structure disappears completely because almost all polaritons are now in or close to the ground state in terms of energy and momentum. This allows us to reliably obtain information about the temporal coherence properties of the condensate by determining the first-order temporal correlation function $g^{(1)}(t) \equiv g^{(1)}(0, 0; t)$ which is plotted for different pumping powers in Fig. S6(b). The measured dephasing time is on the order of 1-2 ps, shorter than the polariton lifetime, and it seems to become slightly shorter for higher pumping powers.

The dephasing time of the condensate in our system is most likely limited by intensity fluctuations of the pumping laser since much longer dephasing times have been observed with the same sample [6] and in other experiments [7] when using single-mode lasers. Fluctuations in the particle number lead to changes of the ground state energy because of repulsive polariton-polariton interactions and therefore destroy phase coherence [8]. Assuming a Gaussian distribution of the energy fluctuations $g^{(1)}(t)$ can be calculated using the Kubo stochastic line-shape theory:

$$g^{(1)}(t) = \exp\left(-\frac{2\tau_r^2}{\tau_c^2}\left(e^{-t/\tau_r} + \frac{t}{\tau_r} - 1\right)\right) \quad (2)$$

where τ_r describes the time scale of the fluctuations and τ_c the width of the energy fluctuations. The above equation can also be derived using a quantum model of the polariton condensate [8]. The predicted form of $g^{(1)}(t)$ is Gaussian for $t \ll \tau_r$ and exponential for $t \gg \tau_r$. Fits of equation (2) to our experimental data (see Fig. S6(b) and Table 1) give $\tau_r \sim 0.3 - 2.0$ ps and $\tau_c \sim 1$ ps. τ_c seems to be approximately constant, whereas τ_r increases with increasing pumping power.

In Fig. 4(c) of the main text, we plot the exponent a_p of the power law fit $(\lambda_p/\Delta x)^{a_p}$ of the correlation function $g^{(1)}(\Delta x)$.

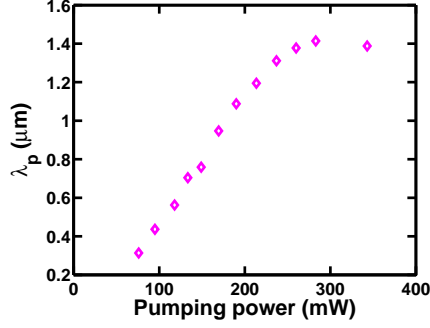


Figure S7: Parameter λ_p from the power law fit of the correlation function $g^{(1)}(\Delta x) = (\lambda_p/\Delta x)^{a_p}$ at long distances Δx .

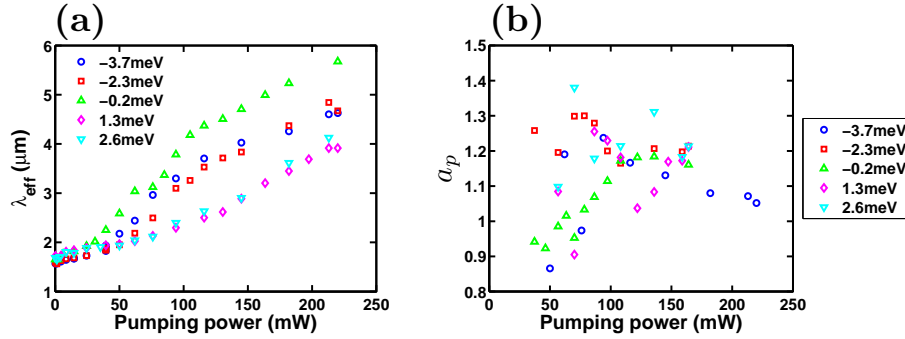


Figure S8: (a) Effective thermal de Broglie wavelength λ_{eff} as a function of laser pumping power for several photon-exciton detunings δ . The prism is in the horizontal orientation. (b) Exponent a_p of the power law decay as a function of laser pumping power. In both figures, data for $\delta = -0.2 meV$ are reproduced from the main text.

In Fig. S7, we plot the parameter λ_p of the same fit. Although λ_p has units of length, it is not a characteristic length of the system. In equilibrium BKT theory, the long-distance decay of $g^{(1)}(\Delta x)$ is of the form [9]

$$g^{(1)}(\Delta x) = \frac{n_s}{n} \left(\frac{\xi}{\Delta x} \right)^{1/(n_s \lambda^2)}, \quad (3)$$

where n_s is the superfluid density, n is the total density, ξ is the healing length and λ is the thermal de Broglie wavelength. In this notation, $\lambda_p = \left(\frac{n_s}{n} \right)^{n_s \lambda^2} \xi$. Thus, as the density is increased above the critical density, the superfluid fraction n_s/n increases, and λ_p increases accordingly. This behavior is qualitatively reproduced by our experimental results in Fig. S7.

Thanks to the wedged sample shape, moving to a different position on the same sample shifts the cavity resonance. This way, we can control the energy difference (detuning) between the cavity and exciton resonances. We have repeated the measurements reported in the main text at several photon-exciton detunings δ in the range $-3.7 meV \leq \delta \leq 2.6 meV$ (corresponding to effective mass $7.8 \times 10^{-5} \leq \frac{m^*}{m_e} \leq 11.5 \times 10^{-5}$). The results are summarized in Fig. S8. In Fig. S8(a), we plot the experimental results for the effective thermal de Broglie wavelength λ_{eff} as a function of pumping power, the same quantity that is plotted in Fig. 2(b) of the main text. The behavior is similar for all detunings, and the qualitative explanation

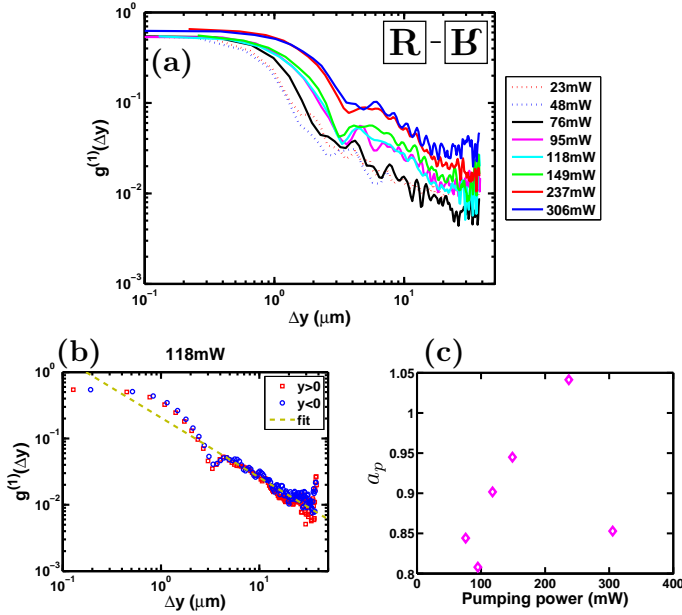


Figure S9: Same as Fig. 4 of the main text, but now the prism of the Michelson interferometer is in the vertical orientation. (a) $g^{(1)}(\Delta y) = g^{(1)}(|2y|) \equiv g^{(1)}(y, -y)$ vs Δy for increasing laser power. The laser pumping spot radius is $R_0 = 19\mu\text{m}$ and the threshold power $P_{th} = 55\text{mW}$. (b) $g^{(1)}(\Delta y)$ vs Δy for one particular laser power and for y both positive (blue circles) and negative (red squares). Dashed line is a power law fit. (c) Exponent a_p of the power law decay as a function of laser power.

is given in the main text. The measured λ_{eff} takes about the same values for all detunings at very low pumping power, as the measurement is resolution-limited in this region. In Fig. S8(b), we plot the fitting results for the exponent a_p of the power law decay of $g^{(1)}(\Delta x)$ at long distances. The same quantity is plotted in Fig. 4(c) of the main text for $\delta = -0.2\text{meV}$. The long-distance decay was indeed found to be a power law, with an exponent in the range $0.9 - 1.3$ when including different detunings.

In [1], it was shown that vortex-antivortex pairs are produced at the center of our condensate, and move inside it before recombining. Because of a small asymmetry of the pumping spot, they always sit along the horizontal axis. For an appropriately small condensate, there is on the average only one vortex pair inside the condensate at any time, and it can be observed with a Michelson interferometer measurement using the vertical prism orientation, for which points (x, y) interfere with $(x, -y)$. Although the pair is mobile, so that the vortex and antivortex follow a correlated motion, a characteristic phase pattern is present in the interferogram. In the horizontal prism orientation, points (x, y) interfere with $(-x, y)$, so the vortex in (x, y) overlaps with the antivortex in $(-x, y)$ and no phase defects appear on the interferogram. The single pair is observed for pumping spot radius of $12\mu\text{m}$. For the $22\mu\text{m}$ spot radius that we currently use, we expect several pairs to be present, so that no clear signature of them can be witnessed in the interferograms. Because of the vortex pair motion inside the condensate, though, $g^{(1)}(y, -y)$ takes smaller values than $g^{(1)}(x, -x)$.

In Fig. 2(b) of the main text we showed that in the vertical prism orientation the effective de Broglie wavelength is shorter than in the horizontal prism orientation. We now compare the long-distance behavior of $g^{(1)}(r)$ between the two cases. In Fig. S9, we plot the same quantities as Fig. 4 of the main text, but now the prism orientation is vertical, so we interfere points (x, y) with $(x, -y)$, instead of (x, y) with $(-x, y)$. In Fig. S9(a), we plot the measured correlation function

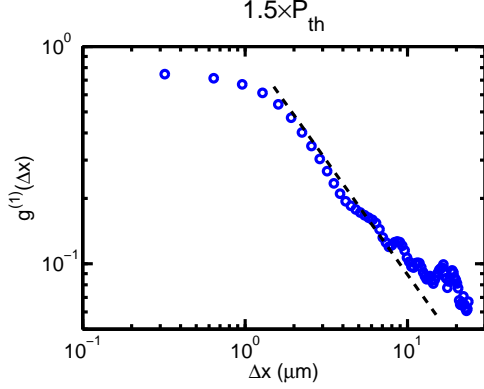


Figure S10: Measured correlation function (blue circles) under singlemode laser excitation and energy-integrated detection. The diameter of the pumping spot is $12\mu m$, and the pumping power is $1.5 \times P_{th}$. The dashed line is a power law decay with exponent of 1.05.

$g^{(1)}(\Delta y) = g^{(1)}(2|y|) \equiv g^{(1)}(y, -y)$ versus Δy for several pumping powers. As in Fig. 4(a) of the main text, phase coherence is extended above the condensation threshold. In Fig. S9(b), we plot $g^{(1)}(\Delta y)$ as a function of Δy for one particular pumping power above threshold. The decay at short distances is more abrupt than in Fig. 4(a), and there is a local minimum at $\Delta y \sim 3\mu m$. But the long-distance decay is again a power law, and the exponent a_p , as shown in Fig. S9(c), is around 1.

To investigate the effect of laser noise, we measured $g^{(1)}(\Delta x)$ under singlemode laser excitation and energy-integrated detection. We again found a power law dependence at large distances, as shown in Fig. S10. This suggests that the power law behavior is not influenced much by the laser intensity noise, but is rather inherent to the pump and decay processes in the microcavity. Due to the limited power of our singlemode laser, we could not study larger condensates, but the power law dependence is already clear at this condensate size.

Finally, we studied an identical sample at a temperature of 200K, and an area where the cavity resonance is above the bandgap. At this temperature, excitons are dissociated, and only standard lasing is possible. We use ps pulsed excitation at a large angle and a wavelength $\lambda = 746.1nm$. The pumping spot was gaussian with diameter $\sim 25\mu m$. In Fig. S11, we show the measured spectrum and total luminescence intensity as a function of pumping power. A lasing transition is observed above $70mW$. We measured $g^{(1)}(x, -x)$ above threshold (Fig. S12), and found that it decays exponentially above threshold. This data suggests that the interactions of the strongly coupled exciton-polaritons are essential in the observation of the reported phenomena.

2 Theoretical model of power law decay

This section expands the discussion of correlations for a non-equilibrium polariton condensate, making use of the formalism presented in [10, 11]. We discuss in more detail the two cases presented in the article, that of a thermalised system, where the equilibrium exponent is recovered, and that of a noisy system, where a different exponent is recovered.

For a two-dimensional Bose gas, where long distance coherence is dominated by phase fluctuations, the asymptotic form

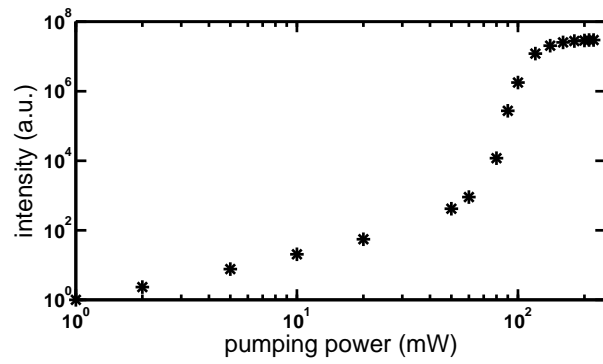
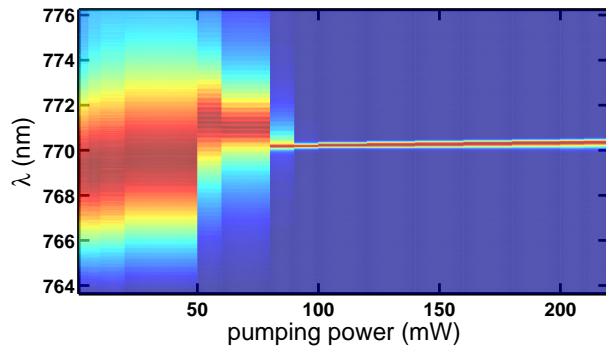


Figure S11: High-temperature data (200K). The measured spectrum (top) and luminescence intensity (bottom) as a function of pumping power. The lasing frequency is above the bandgap, so this is a standard lasing phenomenon.

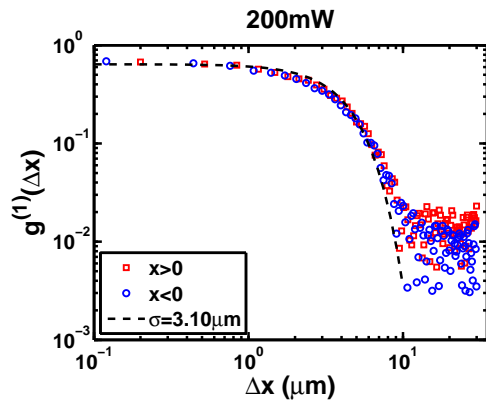


Figure S12: High-temperature data (200K). Measured $g^{(1)}(x, -x)$ above threshold. $g^{(1)}$ decays exponentially until it hits the experimental noise floor of ~ 0.01 . The black dashed line is a gaussian fit. Compare with Fig. 6(b) of the main text.

of the correlation function can be written as:

$$g_1(\Delta x) = n_{\text{QC}} \exp \left\{ - \int \frac{kdk}{2\pi} [1 - J_0(k\Delta x)] f(k) \right\} \quad (4)$$

where n_{QC} is the quasi-condensate density, $J_0(k\Delta x)$ is a Bessel function, resulting from angular integration, and $f(k) = \int (d\omega/2\pi) iD_{\phi\phi}^<(k, \omega)$, where $D_{\phi\phi}^< = D_{\phi\phi}^K - D_{\phi\phi}^R + D_{\phi\phi}^A$ is the phase-phase component of the Green's function corresponding to emission.

The Green's functions $D^{K,R,A}$ are the Keldysh, retarded, and advanced Green's functions, which together define the density of states for fluctuations, and the occupation of those states in the non-equilibrium system. In order to calculate $f(k)$, it is necessary to know the full form of the Green's function, and not just the excitation spectrum. This is because it is necessary to distinguish those excitations that correspond to phase fluctuations from those that correspond to density fluctuations.

The Keldysh Green's function can be found by combining the retarded and advanced Green's functions with the inverse Keldysh Green's function $[D^{-1}]^K$. The inverse Keldysh Green's function describes the noise, due either to thermal excitations or pumping noise, which leads to the occupation of the phase modes. The Keldysh Green's function then has the form $D^K = -D^R[D^{-1}]^K D^A$. This can be thought of as a generalisation of the fluctuation-dissipation theorem, as the retarded and advanced Green's functions encode dissipation, the Keldysh Green's function D^K describes the fluctuations, and so $[D^{-1}]^K$ encodes the relation between these.

In the following, we first summarise previous results for the retarded and advanced Green's functions, and then discuss the two cases presented in the article for the Keldysh Green's function.

2.1 Retarded and Advanced Green's functions: Density of states

Since the long wavelength form of the Green's function is independent of details of specific models, the retarded Green's function can be derived in many ways. One intuitive approach is to consider the linear response of order parameter equation of a non-equilibrium condensate, the complex Gross-Pitaevskii Equation,

$$i\partial_t \psi = \left[-\frac{\hbar^2 \nabla^2}{2m} + U|\psi|^2 + i(\gamma - \Gamma|\psi|^2) \right] \psi. \quad (5)$$

Following standard methods [12], this gives a Green's function which may be written in the ψ, ψ^\dagger basis as:

$$D^R = \frac{1}{\omega^2 + 2i\gamma\omega - \epsilon_k(\epsilon_k + 2\mu)} \begin{pmatrix} \mu + \epsilon_k + \omega + i\gamma & -\mu + i\gamma \\ -\mu - i\gamma & \mu + \epsilon_k - \omega - i\gamma \end{pmatrix}, \quad (6)$$

in which $\epsilon_k = \hbar^2 k^2 / 2m$ is polariton dispersion at long wavelengths. The phase-phase component can be found by changing to the density-phase basis [11]. In terms of the ψ, ψ^\dagger basis matrix structure, the phase-phase component is thus:

$$iD_{\phi\phi} = \frac{i}{8n_S} (1 \ -1) D \begin{pmatrix} 1 \\ -1 \end{pmatrix}. \quad (7)$$

2.2 Thermalised case

As discussed above, for the thermalised case, the form of the inverse Keldysh Green's is fixed by the fluctuation dissipation relation. In the ψ, ψ^\dagger basis, the matrix structure (see [11]) requires $D_{\psi\psi^\dagger}(\omega) = -D_{\psi^\dagger\psi}^*(-\omega)$ so the distribution can be written

$$[D^{-1}]^K = 2i\gamma \coth\left(\frac{\omega}{2k_B T}\right) \begin{pmatrix} 1 & 0 \\ 0 & -1 \end{pmatrix}. \quad (8)$$

We will focus only those terms which lead to the power law decay, and ignoring those that only affect short range correlations¹. Expanding the Green's function for low frequencies and long wavelengths (i.e. considering the terms that control the asymptotic behaviour at large distances), one then finds:

$$iD_{\phi\phi}^< \simeq \frac{4\gamma\mu k_B T}{n_S |\omega^2 + 2i\gamma\omega - \epsilon_k(\epsilon_k + 2\mu)|^2}. \quad (9)$$

After integrating Eq. (9) over ω , the final expression does not depend on γ , and so the modified spectrum has no effect on the exponent when the system is thermalised. Thus, one has:

$$\int \frac{d\omega}{2\pi} iD_{\phi\phi}^< \simeq \frac{\mu k_B T}{n_S \epsilon_k(\epsilon_k + 2\mu)} \simeq \frac{m k_B T}{n_s \hbar^2 k^2}. \quad (10)$$

Then, performing the integral over k in Eq. (4), there is a logarithmic divergence $\int k dk/k^2$, which is cut off for $k < 1/\Delta x$ by the numerator $1 - J_0(k\Delta x) \rightarrow 0$. Thus, one recovers the standard form $g_1(\Delta x) \propto \exp(-a_p \ln(\Delta x))$ with the equilibrium result $a_p = m k_B T / 2\pi n_s \hbar^2$.

2.3 Noisy case

To model a non-thermalised system with excess noise, one may note that the inverse Keldysh Green's function can also be interpreted as the spectrum of noise the system experiences, arising due to pumping and decay (see e.g. [13]). Thus, taking a flat (i.e. Markovian) noise correlation function, with strength ζ , one has:

$$[D^{-1}]^K = 2i\zeta \begin{pmatrix} 1 & 0 \\ 0 & 1 \end{pmatrix}. \quad (11)$$

Because this corresponds to a frequency independent noise strength ζ , the matrix structure is different from Eq. (8). In the same way as above, we may calculate the part of $D_{\phi\phi}^<$ which dominates at long distances, which leads to the expression:

$$iD_{\phi\phi}^< \simeq \frac{2\zeta(\mu^2 + \gamma^2)}{n_S |\omega^2 + 2i\gamma\omega - \epsilon_k(\epsilon_k + 2\mu)|^2}. \quad (12)$$

This expression clearly has identical ω and k dependence to Eq. (9), thus the integration follows in exactly the same way. The difference between the two expressions corresponds purely to replacing $k_B T \rightarrow \zeta \frac{\mu^2 + \gamma^2}{2\mu\gamma}$, hence the modified exponent, $a_p = \frac{\mu^2 + \gamma^2}{2\mu\gamma} m\zeta / 2\pi n_s \hbar^2$. Considering the model nonlinear pumping written in Eq. (5), the density, and hence blueshift, are set by the net pumping strength $\mu = \gamma U / \Gamma$, thus the only pump power dependence of the exponent a_p comes from $a_p \propto \zeta / n_s$.

¹In fact, it is only the contribution from D^K which is responsible for the power law decay at long distances; the contribution from $D^R - D^A$ is finite at long distances, and so just provides a constant prefactor for the correlation function.

References

- [1] G. Roumpos, M. D. Fraser, A. Löffler, S. Höfling, A. Forchel, and Y. Yamamoto (2011), Single vortex-antivortex pair in an exciton polariton condensate. *Nature Phys.*, 7: 129–133.
- [2] M. Richard, J. Kasprzak, R. Romestain, R. André, and L. S. Dang (2005), Spontaneous coherent phase transition of polaritons in CdTe microcavities. *Phys. Rev. Lett.*, 94: 187401.
- [3] M. Wouters, I. Carusotto, and C. Ciuti (2008), Spatial and spectral shape of inhomogeneous nonequilibrium exciton-polariton condensates. *Phys. Rev. B*, 77 : 115340.
- [4] E. Wertz, L. Ferrier, D. Solnyshkov, R. Johne, D. Sanvitto, A. Lemaître, I. Sagnes, R. Grousson, et al. (2010), Spontaneous formation and optical manipulation of extended polariton condensates. *Nature Phys.*, 6: 860–864.
- [5] A. M. Weiner. *Ultrafast optics* (John Wiley & sons, 2009).
- [6] G. Roumpos, W. H. Nitsche, S. Höfling, A. Forchel, and Y. Yamamoto (2010), Gain-induced trapping of microcavity exciton polariton condensates. *Phys. Rev. Lett.*, 104 : 126403.
- [7] A. P. D. Love, D. N. Krizhanovskii, D. M. Whittaker, R. Bouchekioua, D. Sanvitto, S. A. Rizeiqi, R. Bradley, M. S. Skolnick, et al. (2008), Intrinsic decoherence mechanisms in the microcavity polariton condensate. *Phys. Rev. Lett.*, 101 : 067404.
- [8] D. M. Whittaker and P. R. Eastham (2009), Coherence properties of the microcavity polariton condensate. *EPL*, 87: 27002.
- [9] Z. Hadzibabic and J. Dalibard (2009), Two-dimensional bose fluids: An atomic physics perspective. [arXiv:0912.1490v2](https://arxiv.org/abs/0912.1490v2) [cond-mat.quant-gas].
- [10] M. Szymańska, J. Keeling, and P. Littlewood (2006), Nonequilibrium quantum condensation in an incoherently pumped dissipative system. *Phys. Rev. Lett.*, 96 : 230602.
- [11] M. Szymańska, J. Keeling, and P. Littlewood (2007), Mean-field theory and fluctuation spectrum of a pumped decaying bose-fermi system across the quantum condensation transition. *Phys. Rev. B*, 75 : 195331.
- [12] L. P. Pitaevskii and S. Stringari. *Bose-Einstein Condensation* (Clarendon Press, Oxford, 2003).
- [13] A. Kamenev. Many-body theory of non-equilibrium systems. In H. Bouchiat, Y. Gefen, S. Guéron, G. Montambaux, and J. Dalibard, editors, *Nanophysics: Coherence and transport, Les Houches*, volume LXXXI, p. 177 (Elsevier, Amsterdam, 2005).